

## Accepted Manuscript

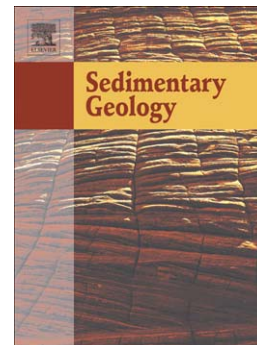
Internal deformation and kinematic indicators within a tripartite mass transport deposit, NW Argentina

Matheus S. Sobiesiak, Ben Kneller, G. Ian Alsop, Juan Pablo Milana

PII: S0037-0738(16)30032-X  
DOI: doi: [10.1016/j.sedgeo.2016.04.006](https://doi.org/10.1016/j.sedgeo.2016.04.006)  
Reference: SEDGEO 5040

To appear in: *Sedimentary Geology*

Received date: 27 October 2015  
Revised date: 25 March 2016  
Accepted date: 11 April 2016



Please cite this article as: Sobiesiak, Matheus S., Kneller, Ben, Alsop, G. Ian, Milana, Juan Pablo, Internal deformation and kinematic indicators within a tripartite mass transport deposit, NW Argentina, *Sedimentary Geology* (2016), doi: [10.1016/j.sedgeo.2016.04.006](https://doi.org/10.1016/j.sedgeo.2016.04.006)

This is a PDF file of an unedited manuscript that has been accepted for publication. As a service to our customers we are providing this early version of the manuscript. The manuscript will undergo copyediting, typesetting, and review of the resulting proof before it is published in its final form. Please note that during the production process errors may be discovered which could affect the content, and all legal disclaimers that apply to the journal pertain.

## **Internal deformation and kinematic indicators within a tripartite Mass Transport Deposit, NW Argentina.**

Matheus. S. Sobiesiak<sup>1</sup>, Ben Kneller<sup>1</sup>, G. Ian Alsop<sup>1</sup>, Juan. Pablo. Milana<sup>2</sup>

<sup>1</sup> Dept. of Geology and Petroleum Geology, University of Aberdeen, Aberdeen AB24 3UE, Scotland, U.K.

<sup>2</sup> Universidad Nacional de San Juan, Mitre Este, San Juan, Argentina

### **Corresponding author.**

E-mail addresses: matheus.sobiesiak@gmail.com (M.S. Sobiesiak), b.kneller@abdn.ac.uk (B. Kneller), ian.alsop@abdn.ac.uk (G.I. Alsop), [jpmilana@gmail.com](mailto:jpmilana@gmail.com) (J.P. Milana).

### ***Abstract***

The role of Mass Transport Deposits (MTD's) in redistributing sediment from the shelf-break to deep water is becoming increasingly apparent and important in the study of basins. While seismic analysis may reveal the general morphology of such deposits, it is unable to provide information on the detailed geometry and kinematics of gravity-driven transport owing to the limits of seismic resolution. Outcrop analysis of ancient MTD's may therefore provide critical observations and data regarding the internal deformation and behaviour during slope failure. One such field area where geometry and kinematics are clearly exposed is Cerro Bola in the Paganzo basin of northwestern Argentina. This 8 km strike section exposes a mid to late Carboniferous succession, comprising fluvio-deltaic sediments, turbidites and MTDs. Our work focuses on the main MTD that is up to 180 m thick and is characterized by a silty matrix, containing sandstone blocks and siltstone rafts. Although we consider a single slope failure as the most likely scenario, a possible double failure might also explain the occurrence of a folded turbidite marker in the upper zone of the MTD. The MTD is host to a variety of deformational features such as folding, boudinage, shear zones, allochthonous strata, and secondary fabrics among others. These deformational features vary in intensity, scale and style, both vertically

and laterally across the deposit. The vertical variation is the most notable, and the entire deposit can be subdivided into lower, middle and upper zones according to variations in texture and structures, including sandstone blocks, sand streaks and blebs in the matrix, folding on a variety of scales, and shear zones. The middle part of the MTD is characterized by the abundance of siltstone rafts. Various models are proposed for the origin of blocks and rafts within the MTD: erosion of underlying strata; fragmentation of the original protolith; or a mixture of both. Significantly, specific strain cells occur around the blocks, and so the kinematics of deformation structures in the matrix of the MTD are very largely governed by their proximity and position relative to blocks, and may not relate to the overall kinematics of the MTD. This casts serious doubt on the ability to interpret overall movement directions from core or dip-meter data in the subsurface.

**Keywords:** Mass-Transport Deposit, Siltstone Rafts, Sandstone Blocks, Carboniferous, Argentina, Late Paleozoic Ice Age

## 1 Introduction

Gravity-driven processes resulting in blocks or megaclasts are increasingly recognized as a consequence of slope failure and instability from modern and ancient deep-water sedimentary basins (e.g. Alves and Cartwright, 2009; Alves, 2015; Dunlap et al., 2010; Jackson, 2011; Lee et al., 2004; Macdonald et al., 1993; Moscardelli and Wood, 2015) and even in Mars (Moscardelli, 2014). They are considered to be a major contributor to the transfer of sediments from the shelf break to deep water, and commonly represent between 50% to 90% of the deep-water stratigraphic succession (Garziglia et al., 2008; Newton et al., 2004; Posamentier and Martinsen, 2011). Submarine gravity-driven processes are very complex and comprise creep, slide, slump, debris flow and multiphase granular flows. The remobilised sedimentary deposits resulting from these processes are termed mass transport deposits (MTDs) or mass transport complexes (MTCs). Non-cohesive flows, such as turbidity currents, while also being gravity flows, are not included in the terminology mentioned above.

Blocks within MTDs are characterized by their internal coherence and can be found undeformed to moderately deformed, with their size and shape varying greatly, dependent on their location within the MTD, and also from one deposit to another. According to the literature (e.g. Bull et al., 2009), blocks within MTDs can be subdivided into remnants and rafts. Remnant blocks are considered as “isolated blocks of material that have not experienced failure” (Bull et al., 2009). They are normally bound by sets of faults with a lack of basal disruption and vertical continuity with the substrate, (Alves and Cartwright, 2009). Rafts, which are sometimes also called ‘translated’ or ‘intact’ blocks, behave as “coherent blocks of sediment that have been transported within or in front of the failed mass and are often deposited within the translational domain” (Bull et al., 2009).

In this manuscript, we use the same criteria that (Alves, 2015) employed to define blocks or megaclasts, which is anything bigger than boulder size ( $>4,1$  m) (Blair and McPherson, 1999). We only describe individual blocks that were transported within the MTD and are therefore ‘floating’ within the matrix. Additionally these translated blocks are defined herein as (i) blocks; that are



transported fragments of sandy material different from the matrix; and (ii) rafts; that are transported fragments of silty strata similar to the matrix (Fig.1).

Soft-sediment deformation (SSD) occurs during or after sediment deposition, and describes deformational structures developed in unconsolidated sediments, or in sedimentary rocks that were not yet lithified (Brodzikowski and van Loon, 1987; Maltman, 1984; Mills, 1983; Van Loon, 2009). Thus, MTDs are known to host a wide variety of SSD structures, many of which resemble those developed in metamorphic rocks (Butler and McCaffrey, 2010; Strachan and Alsop, 2006). Such structures can be used to evaluate the degree and style of internal deformation within both the blocks and the matrix, thereby aiding in the assessment and classification of different deformational zones (Alves, 2015).

The aim of this paper is to document the sedimentology of a MTD, and in particular to emphasise the different types and styles of SSD structures and kinematic indicators within the deposit. We have chosen a particularly well exposed MTD in NW Argentina for our case study, which enables us to provide detailed descriptions and measurements, demonstrate how deformation styles and geometry change vertically, how heterogeneous blocks can be, and how they affect and are affected by flow in the MTD matrix. In addition, we propose a mechanism for the emplacement of this MTD.

## **2 Geological Setting**

Cerro Bola is a mountain located at the south-western border of La Rioja and San Juan Provinces, near the town of Guandacol, western Argentina. The sedimentary succession at Cerro Bola represents the western margin of the Late Paleozoic Paganzo Basin (Fig 2 a and b) (Gulbranson et al., 2010), that extends over an area of 30,000 km<sup>2</sup>, and provides accommodation space for up to ~4500m of sediments (Buatois and Mangano, 1995; Fernandez-Seveso and Tankard, 1995). This glacially influenced basin is the result of the consolidation of Gondwana between the Ordovician and early Carboniferous, and is bounded to the north by the Alto de La Puna and to the south and east by the Pampean and Pie de Palo highs (Limarino et al., 2006).

Deposition in the Paganzo Basin initiated in the early Carboniferous (Fernandez-Seveso and Tankard, 1995) and continued until the middle to late Permian, and was therefore affected by the Late Carboniferous glaciation. Regionally the oldest rocks lie unconformably on Ordovician limestones and Precambrian metamorphic rocks that represent the basin margins. Limarino et al., (2002) separated the basin into western, central and eastern domains according to postglacial facies associations. In the western domain, the sedimentation style represents an open marine setting and changes to a more brackish setting in the eastern domain. The central domain forms the transition between these two settings and includes the Cerro Bola area. The Paganzo Group is divided lithostratigraphically into three super-sequences (Fernandez-Seveso and Tankard, 1995): Guandacól, Tupe and Patquía. The Guandacól super-sequence, which comprises the deposits described here, has an overall thickness at Cerro Bola of ~1825m including turbidites, shales, MTDs and fluvio-deltaic sandstones containing drop-stones.

Structurally, Cerro Bola (Fig 2 c) consists of a large north-south trending west-vergent periclinal anticline that forms the hanging-wall to a thrust system that dips eastward at ~ 24°. The thrust system is related to the Late Tertiary to Quaternary Pampean Range orogenic deformation (Zapata and Allmendinger, 1996). The whole sedimentary succession of Cerro Bola has a total thickness of 1 km, exposing rocks from the Carboniferous (Guandacól Fm.) to Permian terrestrial red beds (Dykstra et al., 2011; Milana et al., 2010). The Guandacól Fm was affected by the second episode of glaciation during the late Carboniferous (Lopez Gamundi et al., 1990) where glacio-marine sediments were being deposited. The deposits alternate between fluvio-deltaic sediments, mass transport and turbidite intervals (Dykstra et al., 2011; Milana et al., 2010), and record at least three major glacial/deglacial cycles (Fallgatter, 2015; Valdez Buso, 2015) and several minor transgressive-regressive successions (T-R), which are ascribed to an unconfined depositional setting (Fig 2 d). These three cycles each consist of a shallowing-upwards succession around 200-400m thick (Dykstra et al., 2011; Milana et al., 2010) (Fig 2 d).

The first cycle has an overall thickness of 200 m, and comprises a fluvio-deltaic sequence (FDI) overlain by a MTD (MTDI). The second cycle has an overall thickness of 440 m and is composed of a fluvio-deltaic unit (FDII), overlain by the main MTD (MTDII) with sandstone blocks (the focus of

this study). This in turn is overlain by ponded turbidites, black shales (maximum flooding zone), and turbidite sandstones, ending in another fluvio-deltaic unit. The third cycle has an overall thickness of 375 m and comprises an MTD (MTDIII) with a rugose upper surface that locally is infilled with sandstone (probably turbidites), overlain by a thin mudstone unit, turbidite sandstone unit, fluvio-deltaic unit and then Permian red beds (Dykstra et al., 2011; Milana et al., 2010) (Fig 2 d).

The evidence that MTDII was emplaced directly onto a surface that was formed at or close to sea level (i.e. the top of the fluviodeltaic secession), and is itself overlain by turbidites requires a change in relative sea level that is significantly greater than the thickness of the MTD (up to 180m). The magnitude of Late Paleozoic glacio-eustatic sea level changes is of the order of 100 m (Ross and Ross, 1985; Rygel et al., 2008), insufficient to accommodate the MTD, still less maintain the water depths to allow turbidite sedimentation. It seems therefore that there must have been significant tectonic subsidence between deposition of the fluvio-deltaic unit FDII and emplacement of MTDII. This implies the passage of a substantial period of time (at least hundreds of thousands of years) between deposition of the two units.

### **3 Overview of MTD II**

Cerro Bola exposes a strike section of the Paganzo Basin with excellent two and three-dimensional exposure. The MTD outcrop is up to ~180 m thick and 8 km in length, and forms a doubly-plunging anticline with a steeply dipping western limb (close to the hinge area) and a gently-dipping eastern limb. The MTD generally consists of a green, highly sheared, fine-grained (silt size) matrix of remobilized sediments, with granule to boulder-sized clasts composed of coarse-grained granitoid and metamorphic basement rocks. These clasts have high sphericity, are sub- to well rounded, and display striated surfaces in some cases. They are indicative of reworking and are interpreted as drop-stones associated with ice-rafted debris (IRD) (Fig 3 a, b). Other clasts found within the matrix include dark mudstone and thin-bedded turbidites. We therefore interpret the 'protolith' of the MTD to be glaciogenic sediments derived from floating ice. The granitoid and metamorphic drop-stones are considered to be sourced from the highlands that surround the Paganzo

basin, which would include the proto-Precordillera to the west, Sierras Pampeanas to the east and Alto de La Puna to the north.

One of the distinguishing characteristics of the MTD is the abundance of ball-shaped nodules embedded within the matrix, which provide the name (Bola) of the mountain. These balls are silica-cemented concretions that in most cases developed around a pebble (drop-stone) (Fig 3 c and d). The majority of the concretions are sub-rounded, while a small percentage (~ 2%) form ellipsoidal bodies that are flattened parallel to the bedding. Whether the concretions are pre- or post-remobilisation is difficult to determine since there is no sign of matrix deflection around them. Any variations in their shape (round or flattened) is therefore attributed to the growth habit rather than subsequent deformation.

A second significant characteristic of the MTD is the presence of blocks and rafts (Fig 4). The blocks are considered to represent transported fragments of sandy material that exhibit a different rheological behaviour from the matrix. Their margins display shearing and/or other deformational features caused by the flow (see section 4 and 5.1). Rafts represent fragments of silty strata similar to the matrix, and thus have a similar rheology to the matrix and are weakly deformed by the flow.

Rafts and blocks are each divided into three different types, according to their lithological characteristics.

Blocks are divided into:

- a) sandstone blocks.** These are whitish to orange, relatively homogeneous and composed of medium- to coarse-grained, moderately sorted arkosic sandstone. They are highly fractured, commonly displaying a massive internal structure, but occasionally preserving primary features such as cross-stratification and trough cross bedding, ripples, climbing ripple and cross-lamination (Fig 4 a).
- b) dirty sandstone blocks.** These are light grey in colour, composed of fine- to medium grained sand, and have a matrix of silt sized mud and mica (>5%). They possess rectangular shaped mud chips that can vary from mm to 10 cm in length, and mm to 3 cm in thickness (Fig 4 b).
- c) folded turbidite.** These are isolated, generally folded, dark orange to black 1 – 1.5 m thick sandstone beds comprising poorly sorted sand displaying normal grading. They are occasionally accompanied by a thick ~1m mudstone cap (interpreted as a “mega-bed”) (Fig 4 c).

Rafts are divided into:

**d) *bedded siltstones with drop-stones.*** This is a light to dark green layered rock, with each layer ranging in thickness from mm up to 10 cm of silt, dark mud and sandstone. Clasts are randomly intercalated, and range from granules to boulders (drop-stones). The layers below and above the clasts are deflected around them. These rafts display a low degree of internal deformation (Fig 4 d).

**e) *bedded siltstones;*** This unit has similar characteristics to the rafts above (d), but contains no clasts (drop-stones). They consist of light to dark green silt, dark mud, and sandstone layers that range from mm to 10 cm in thickness, and display a low degree of internal deformation (Fig 4 e).

**f) *massive siltstone blocks.*** These range from light to dark green in colour and resemble the host MTD. They are homogeneous fine grained (silt size), and highly fractured with massive internal structure (Fig 4 f).

The lower and upper boundaries of the MTD are extremely irregular (Fig 5), with the irregularities along the upper surface considered to be syn-depositional as suggested by the presence of truncation and onlap of sediments. The basal contact displays groove-shaped depressions and scours of various size, ranging from couple of metres up to hundreds of metres in length and up to ~ 20 m in height. We suggest that these features mark erosion and/or deformation related to translation of the MTD. The topography formed on top of a MTD is determined by the combination of the dynamics of the initial flow and internal structure of the final deposit, together with the geometry of the basal surface (Dykstra et al., 2011; Kneller et al., 2016; Milana et al., 2010). In the case of the main MTD at Cerro Bola, evidence for such topographic irregularity is found in the onlap of the turbiditic sediments on top of the MTD (Kneller et al., 2016).

The MTD was first described by Dykstra et al., (2011), who noticed the vertical changes within the deposit and divided it stratigraphically into distinct lower, middle and upper zones according to internal variation in texture and structures (Fig 6 a). The lower zone is characterized by the presence of numerous sandstone blocks (Fig 6 b) and a variably sandy matrix; the middle zone has a silty matrix and the occurrence of siltstone blocks with and without drop-stones; and the upper zone is marked by the presence of thrust zones, large scale folding and imbrication. The contacts between the zones are transitional and we now describe structures from each of these zones in more detail.

## 4 Internal Structure of MTDII

### 4.1 Lower zone of MTDII

As described above, the main distinguishing characteristic of the lower zone (Fig 6) is the presence of sandstone blocks. There is however a range of other features that characterize this zone, such as: sand stringers, blebs and streaks; sand-rich matrix; blocks of siltstone (type d and e); folds; shear zones; compressional zones; and thrust faults.

Sandstone blocks occur throughout the lower zone and locally comprise up to 30% of the MTD exposure. They range in size from a few metres up to ~ 90 m long, and up to ~ 15 m thick (Fig 4 a and 6 b). Although their shape varies substantially, (especially at the bottom of the lower zone) they are often approximately round or eye-shaped, especially on outcrops aligned parallel to the presumed NW-transport direction (Dykstra et al., 2011; Milana et al., 2010). A vertical distribution of blocks is developed in the lower zone, with larger and more irregularly shaped blocks observed at or near the basal shear surface. The blocks are associated with a number of contractional features, such as recumbent folds, which are developed near the margins of the blocks. Blocks are also found imbricating with one another (Fig 7 a) and being thrust upwards into the matrix (Fig 7 b). In comparison, blocks observed higher up the stratigraphy are smaller and eye-shaped (boudin-like). In some cases, it is possible to observe two or three eye-shaped blocks aligned at the same stratigraphic level, and displaying overall 'pinch and swell' geometries.

Fragmentation of the sandstone blocks, together with shear-stripping of their margins are at least two mechanism that introduce sand into the matrix. This suggests that the flow was also interacting with the sandstone blocks in a more abrasive way. This abrasion of the block margins results in a sand-rich matrix, consisting of a quartz rich (~30%) siltstone with varying proportion of crystalline lithic fragments (derived from IRD) (Dykstra et al., 2011). Furthermore, most of the blocks in the lower zone display a heterogeneous mixed streaky halo of sand and MTD matrix extending for up to 2 m from the block, where it merges into the homogeneous sand-rich matrix.

Sand streaks are medium- to coarse-grained, moderately sorted arkosic 'orange' sand. This lithology is similar to the sandstone blocks, and it is notable that the sand streaks become very abundant around sandstone blocks, and diminish away from them, suggesting that sand streaks were derived from abrasion or fragmentation of blocks. The sand streaks were classified into two different types according to their shape and behaviour;

**a) *Sand blebs***; these are chunks of coherent sand similar to the sandstone blocks (type a). They range in size from ~5- to 80 cm in length and up to 40 cm in width, are detached and have undergone shearing (Fig 8 a and b) (Sobiesiak et al., 2016).

**b) *Sand stringers***; these are thin streaks of sand up to ~5 cm thick by 2 to 3 m long. They are distinctly less rigid and appear to be rheologically similar to the matrix. They fade into sand-rich matrix and locally can be mistaken for relic bedding. (Fig 8 c and d) (Sobiesiak et al., 2016). Sand stringers and blebs record a complex deformation history with superimposed compressional and extensional strain histories (Dykstra et al., 2011). They are more common on NE-SW strike sections through the blocks, where the overall bleb kinematics are perpendicular to the main NW-directed flow direction (Dykstra et al., 2011; Milana et al., 2010).

A secondary fabric is noticeable in the lower zone and is marked by sheared planes that are highlighted by composite sand rich horizons that resemble primary bedding. They are interpreted to be the result of shearing generated by flow parallel to the basal shear surface, and may be a reflection of topography along the basal shear surface (Bull et al., 2009).

Siltstone blocks are not very numerous in the lower zone, (mostly types d and e) and where present generally occur as slabs in the upper part of the lower zone. Conversely, they can be found close to the basal shear surface imbricating each other, and against sandstone blocks (Fig 7 a).

Two different types of folds are observed in the lower zone of the MTD that can be broadly subdivided into tectonic and soft-sediment folds. Tectonic folds are distinguished by their scale, folding style, and relationship with other regional and internal structures (e.g. faults, blocks, rafts...). However, the main evidence is their plunge towards the NE, which is subparallel to the hinge of the Cerro Bola anticline, and their position in the axial region and steep limb of this anticline. Soft-sediment folds form prior to lithification of sediments, and may develop by differential flow along

minor detachments during translation of the MTD (Alsop and Marco, 2013). These folds range in size from a couple of centimetres up to tens of metres, but predominantly form on a centimetre scale. They are normally inclined to recumbent cylindrical folds, sometimes displaying superimposed parasitic folds and sheath folds (Fig 8 e and g). The degree of syn-sedimentary folding and faulting in the lower zone is greater than the other overlying zones, probably because the sand-rich-matrix reveals and highlights the structures, which consequently appear more common close to the sandstone blocks.

#### **4.2 Middle zone of MTDII**

The contact between the lower and the middle zones of the MTD is transitional through ~ 15 m and marked by the vertical decrease of sand entrained within the matrix. The middle zone is characterized by a lower sandstone block frequency, and larger amount of siltstone blocks. The matrix is composed of highly fractured green siltstone with drop-stones and very common ball-shaped concretions.

Sandstone blocks in the middle zone are generally smaller and less frequent (comprising up to 5% of the exposure at some localities) than those from the lower zone, but larger blocks measuring up to ~ 30 m long and up to ~ 10 m thick are locally observed. Most of the blocks are eye-shaped, where the long (width) axis is three times greater than the short (height) axis (Fig 1). Blocks may show a flattened shape where the pinched edges are deformed and folded by the flow (Fig 9 a). In addition, some blocks are positioned on top of bedded siltstone rafts (Fig 9 b), where the latter are deformed by, or wrap around, the sandstone blocks. Sand streaks are very scarce in comparison with the lower zone and their occurrence is normally in the form of sand blebs, restricted to the volume immediately surrounding the sand blocks and displaying a complex strain history.

Rafts can be found throughout the middle zone and occur as bedded siltstone both with and without drop-stones, or as massive siltstone. Rafts may be up to ~ 100 m in length by up to ~ 20 m in thickness. The differentiation of the rafts from the matrix can be problematic regardless of their type (d, e and f), since raft and matrix have a similar grain-size and green colour. Additionally, rafts may



show bedded layers that can easily be confused with the matrix fracture sets, while drop-stones can be mistaken for the ball shaped concretions.

The MTD middle zone has tectonic and soft-sediment folds, but their frequency is reduced in comparison with the lower zone. The apparent reduction in fold frequency might simply be due to the lack of markers within the matrix (such as the sand-rich matrix in the lower zone). Soft sediment folds developed in the middle zone have the same deformation style and geometry as those from the lower zone, and are typically inclined, recumbent folds that may also display sheath-type geometries. Folds in this zone are larger, normally up to tens of metres and rarely up to hundreds of metres.

Although shear lozenges are normally found in metamorphic rocks, (e.g. Ponce et al., 2010) similar structures are observed just below two homogeneous sandstone block aligned at the same horizon, hence the sandy matrix. The structure is considered the result of folds that were sheared around the hinge line, leaving only the lower limbs bounded by the shear zone (Fig 10).

### **4.3 Upper Zone of MTDII**

The upper zone is 40 to 60 m thick, well exposed but not as accessible as the lower two zones. The contact between the middle and upper zones is transitional, and marked by the appearance of large-scale folding and fault systems. The matrix remains the same greenish siltstone with drop stones and ball-shaped concretions.

All three types of sandstone blocks are present in the upper zone, but in comparison with eye shaped blocks from the middle zone, are typically scarcer, smaller, and display overall rounded shapes. In addition, the only type b block that can be found in the MTD is located almost on the top of the upper zone. This block is composed of a dirty grey sandstone with aligned mud chips, and has an overall eye shape, similar to the sandstone blocks in the middle zone. An intercalated succession of thin (<5 cm) layers of sandstone and mudstone wrap around the block, and have undergone boudinage, resulting in the sandstone layers pinching and swelling around the sandstone block. All three types of rafts are also present at the upper zone; however, their presence is more limited and they are smaller in comparison with the lower zones.

The folded turbidite (block type c) is developed in the upper zone, and particularly the lower portion of the upper zone. This unit can reach a thickness of 1.5 m, and generally possesses its original mud cap. It therefore represents the deposit of a large single event, making it a 'mega bed'. The turbidite bed is broken into various separate pieces, and those pieces were folded (normally upright and recumbent folds) and refolded during translation. Such pieces are found scarcely distributed throughout the whole length of the outcrop, where they form a useful and traceable marker bed.

Intercalation of bedded silty and muddy layers project upwards in a flame or tongue shaped structure, with a crest that is deflected towards the NW (the inferred transport direction). The structure is ~15 m high by ~7.5 m across and it is interpreted to result from loading and de-watering of water-saturated sediments to create a giant flame structure. The deformed crest of the flame may suggest horizontal drag or movement during translation to the NW (Fig 11).

The main characteristic of the upper zone is the presence of large-scale compressional features such as thrust planes, folds, and shear planes. Folds are found across a wide range of scales, from centimetre up to tens of metres wavelength, and occur throughout the whole zone but are apparently more abundant towards the top of the zone. Folds can be classified as recumbent to upright, curvilinear, sheath and rootless folds, and some can show evidence of up to three different deformation phases. Large-scale folds normally occur above detachment zones (Fig 12 a and 8 h). In addition, folds can be truncated or cut off by sets of detachment planes in the upper part of the zone.

Removal of the effects of the late stage 'tectonic' anticline suggests that slide planes restore to a horizontal or sub-horizontal inclination, and are interpreted to be ramp and flat portions of a thrust system. Such systems display repetition where thrust planes imbricate each other in the inferred transport direction. These systems can be at least 50 m wide by 20 m high comprising no less than five imbricated planes (Fig.12 b). A very well-exposed section (transverse to the main NW transport direction) shows sets of arcuate shaped planes, dipping towards both the north and south, in which some folds are truncated by the planes (Fig.12 c and d). The whole section is ~30 metres thick by ~225 metres long, and the features can be explained as a transverse section through a thrust system with an arcuate shape in plan view (convex in the transport direction; Dykstra et al., 2011).

Alternatively, the thrusts that dip towards the S could be sets of arcuate back thrusts developed by continued compression during translation of the MTD.

Folding in the upper part of the zone has a local and clear influence on the topography generated at the top of the MTD. It is noticeable that topographic highs occur where anticlines are present, and topographic lows are formed above synclines. This relationship is clearly shown by a turbidite that immediately overlies the MTD. The overlain turbidite is interpreted as a co-genetic turbidite for three reasons; (i) is petrographically identical to the MTD, and even display the classic greenish colour that distinguishes the MTD; (ii) the turbidite thickens into the topographic lows on the upper surface of the MTD and thins over the highs (or is even absent on summits) (Fig 8 h); (iii) locally the turbidite slumped from the highs into the lows (Kneller et al., 2016), and this topography was amplified by compaction, deforming the turbidite prior to deposition of the overlying succession.

## **5 Interpretation of MTD features**

### **5.1 Sandstone Blocks**

Sandstone blocks within the MTD can locally comprise up to 35% of the exposure, and their size and shape varies greatly, especially in the lower zone where the vertical variation of the blocks is clear (Fig 6). The largest blocks are commonly preserved at or near the base of the deposit, although it is sometimes difficult to delimit block boundaries due to the limits of exposure. On the other hand, the likelihood of finding original bedding and other sedimentary features (e.g. climbing ripples) are much greater in larger blocks, as the internal deformation is apparently lower. Blocks found higher up the stratigraphy at the top of lower zone and above, tend to have a more pronounced eye shape. Measurements of a block's long axis (x) (lengthwise straight line that crosses the block's midpoint) and short axis (y) (heightwise straight line that intersects the block's midpoint at 90° from long axis) (Fig 1 and 13 a) were acquired, using a measuring tape and on inaccessible areas by photo analysis. It is important to note that although the presence of blocks was obvious, many blocks could not be measured due to exposure. The block's measurements allowed us to calculate the block's aspect ratio and size, showing that the mean block ratio is 3.3:1, ranging from 1.2 to 8.1 (standard deviation of

1.35) (Fig 13 b). Both of these extremes are found in the lower zone, suggesting a great degree of heterogeneity. This suggests that the majority of blocks are boudin-like or eye-shaped, possibly implying extension by flow. This is supported by the occurrence of horizons that display an alignment of two to three eye-shaped blocks (Fig 13 c), which are interpreted as fragments of the same boudinaged block. Additionally the block's aspect ratio can be plotted against their vertical height in the deposit (block's midpoint height is measured upward from the base of the MTD and then normalized to the local thickness, where 1 is the whole thickness of the MTD). Plots demonstrate that the greatest variation in aspect ratio occurs near the base (Fig 13 b). From the middle of the deposit (0.5) upward, the variation in ratios is less than in the lower part of the deposit (2.0 and 4.1). The long and short axis were also plotted against each other (Fig 13 a) and a pattern emerged expressed by a curve that describes the relationship between blocks dimensions, showing that larger blocks have higher aspect ratios, and as the blocks become progressive attenuated, the aspect ratio decreases. In order to evaluate where the described blocks compare with other examples from the literature, we plotted our data against four examples from outcrop and five from the subsurface (Fig 13 d) gathered by (Moscardelli, 2014). Sobiesiak et al., (2016) used our field data to propose a mechanism for the vertical changes in sandstone block size within the MTD. They calculated block's size (square root of block's area) and cross-plotted this against their normalised vertical height (same technique applied for aspect ratio height) (Fig 13 e). The results are that both the mean and maximum block size diminish upwards, and the mean aspect ratio narrows between 3 and 4 towards the top, indicating that blocks were getting progressive smaller and more boudin-shaped towards the top of the flow.

It was proposed by Sobiesiak et al., (2016) that the blocks ascend by buoyancy, due the density contrast between the unlithified and poorly compacted sandstone and the muddy matrix (Joanne et al., 2013). In the process of ascending, blocks get progressive fragmented and extended as they rise through the shearing flow, thus explaining the overall block size distribution within the deposit. However, the presence of small blocks at the lower zone may be due either to the fragmentation of bigger blocks, or that blocks of originally different sizes were being eroded by the flow from the substrate. (Sobiesiak et al., 2016).

## 5.2 Basal Contact (basal shear surface)

As described above, the basal contact of the MTD with the underlying fluvio-deltaic sands is highly irregular, and displays various scours and other erosional features. Such features are clear evidence of basal interaction between the MTD and the underlying sand body. Additionally, sand blocks are most abundant where the basal contact is most irregular. In places it is possible to see proto-blocks, that are interpreted as blocks arrested in the process of erosion by the shearing flow (Fig 14 a). It is believed that the fluvio-deltaic sands were still unlithified at the time the MTD was emplaced, due to the amount of sand stripped from the blocks, together with the amount of centimetre to metre scale folding found within the sands near the basal contact of the MTD. Most of these folds hinges verge towards the NW or WNW. (Dykstra et al., 2011; Garyfalou, 2015; Milana et al., 2010).

A ramp and flat system is believed to occur on the basal shear surface in the northern valley of the MTD, based on the quantity of compressional and deformational features found in both units (MTD and underlying fluvio-deltaic sands), the amount of sand within the MTD (sand streaks, blocks and sand mixed with the matrix), erosional features on the basal contact, and the wide array of long axis inclinations of blocks that dip in a wide variety of directions (Fairweather, 2015). The ramp per se is not clearly distinguishable due to the lack of exposure longitudinally, together with the Cerro Bola anticline structure. However, the ramp system is assumed to have an overall SSW strike with the main transport direction towards the WNW.

## 5.3 Sand Streaks

Sand streaks are interpreted as material sheared or ripped from the sandstone blocks by the flow. Such features would serve as good kinematic indicators if they were controlled by the flow rather than the sandstone blocks themselves. However, the sandstone blocks behave as smaller cells within the MTD, with each secondary flow cell developing its own contractional and extensional domains within which the sand streaks are contained (Alsop and Marco, 2014). When such cells interact with a neighbouring cell, the result is overprinting (Alsop and Marco, 2014). The sandstone blocks seem to have undergone some degree of rotation (Fig 14 b) around their own axes

perpendicular to the main transport direction. This results in sand streaks giving the kinematics of local block rotation rather than of the main flow direction, and as such they may be of limited value in kinematic interpretations.

#### 5.4 Blocks and Rafts:

The origin of blocks and rafts cannot be known with certainty; however, two different scenarios can be proposed based upon the field observation: (1) Single slope failure and (2) Double slope failure (Fig 15).

##### 5.4.1 Single Slope Failure;

In this model, we suggest that the whole of the MTD resulted from a single slope failure. Blocks and rafts within it, could be sourced from three settings (Fairweather, 2015): (1a) erosion of underlying strata (Fig 15 a); (1b) fragmentation of the units originally embedded within the MTD protolith (Fig 15 b); (1c) a mixture of both sources.

Since rafts were defined previously as weakly deformed silty strata that are similar in composition to the matrix, then it follows that due their notable similarity to the matrix, such rafts are the least deformed end member of the protolith (Dykstra et al., 2011; Milana et al., 2010). They resemble slide blocks that have translated downslope with minimum deformation, with most of their original structures preserved intact. This makes any of the scenarios above a good candidate to explain the presence of rafts, and since they are so abundant, their origin is likely to lay within the MTD 'protolith'. However, it is still also possible that some of the rafts were eroded from upslope silty strata, although such *in situ* deposits are nowhere observed.

Blocks might also have a completely different origin. The sandstone blocks (block type a) may have been eroded from the underlying fluvio-deltaic sandstones. This model is supported by the erosional features and irregularities described at the basal shear surface, combined with the soft-sediment deformation structures present within the top-most part of the underlying unit. In addition, the sandstone blocks petrographically resemble the underlying sandstone deposits (Garyfalou, 2015). As with the siltstone rafts, the single dirty sandstone blocks and the turbidite (block type b & c), are

not seen in any similar *in situ* unit, so they might either have been part of the original protolith, or a part of the substrate that was completely removed by erosion beneath the mass movement.

#### 5.4.2 Double Slope Failure;

In this model, we assume that the MTD resulted from two independent failures, in which the first failure deposited the lower and middle zone, followed by the deposition of a co-genetic turbidite, similar to the one present on top of the upper zone (Fairweather 2015, Fallgater 2015, Dykstra 2011, Milana 2010). Subsequently, the first MTD (or similar autochthonous material) fails again, eroding the co-genetic turbidite and depositing a new MTD on top of the first failure (Fig 15 c). Several aspects of the geology support such a scenario including; (i) the turbidite (block type c) could be considered to be the remnants of a remobilized and folded co-genetic turbidite associated with the first failure; (ii) the contact between the middle and upper zone is quite homogeneous and an amalgamation surface could be hidden there; (iii) the change from an extension dominated middle zone to a compressional dominated upper zone may indicate a component of deformation along this contact.

The problems associated with the double failure scenario include; (i) blocks and raft sizes in the upper zone only become smaller compared to the blocks in the middle zone; (ii) the sedimentology of the turbidite is very different from the MTD and from the co-genetic turbidite onlapping the top of the MTD (Kneller et al., 2016).

### 5.5 Kinematic Indicators

The MTD displays a large array of potential kinematic indicators. The complexity associated with the sheared matrix, combined with the amount of rafts and blocks, highlight the necessity to employ more than one single kinematic indicator to designate movement.

#### 5.5.1 Folds;

Folds hinges are one of the most popular and reliable kinematic indicators with which to constrain transport direction (Alsop and Marco, 2012; Woodcock, 1979). However, after plotting several measurements of fold hinges from the MTD, it is apparent that the gently plunging folds are

dispersed in a range of trends and define a rather chaotic distribution (Fig 16 a). This hinge distribution can be explained by the quantity of different blocks and rafts that locally deflects the general flow pattern and thereby affects the behaviour of the slump folding. Despite these concerns, it is noticeable that fold hinges located in the NW sector define a clustered pattern (red circle on Fig 16 a). This grouping of hinges is composed mostly of recumbent folds from the vicinity of sand blocks in the lower zone of the MTD. We interpret these folds hinges as having become detached, thereby allowing their hinges to rotate into parallelism with the main transport direction (see Alsop and Marco, 2013).

#### 5.5.2 Secondary fabric;

Although secondary fabric resembles primary bedding, and is marked by sand rich horizons, it is considered an MTD-related structure that is observed throughout the lower zone. Plotting of the secondary fabric reveals a scatter of data but with a preferential dip towards the southeast (Fig 16 b and c). This configuration could be the result of rotation of the fabric into general parallelism with the lower boundary of the flow, or with local slide surfaces within a ramp and flat system.

#### 5.5.3 Blocks Long Axis (X);

Normally when objects with one axis longer than the other are found within a flow, such objects can be used as a direction indicator. When blocks have been transported for long distances within a flow, they have a tendency to become aligned with their long axis parallel to the flow direction (Bull et al., 2009). The rose diagram on (Fig16 d) shows a compilation of blocks' long axes, and shows a NW-SE orientation, which is consistent with other kinematic and flow indicators.

#### 5.5.4 Ramp and Flat System;

Ramp and flat systems can serve as kinematic indicators under some circumstances and can be used to corroborate other kinematics and the flow direction (Bull et al., 2009). However, ramp and flat systems can be generated perpendicular, oblique and even parallel to the main flow direction, thereby limiting their value as a good indicator. At Cerro Bola it is difficult to define such a system with accuracy.



## 5.6 Vertical Variation

The lower zone of the MTD displays a predominance of simple shear strain. In the upper part of this zone, the behaviour starts to change gradually from simple to pure shear deformation with the occurrence of boudin-like blocks and regular diminishing of sand within the matrix (Fig 17). The middle zone is the least deformed part of the MTD, with low intensity deformational structures displaying extensional behaviour. It seems that it largely translated passively downslope on top of the lower zone as it spread onto the basin floor. Some coherent pieces of the protolith were broken up at weak boundaries by a series of extensional faults. The predominance of rafts in this zone might be governed by a lack of density contrast between the rafts and the matrix combined with the relatively low strain (Fig 17). The upper zone of the MTD displays a contractional style as shown by sets of imbricate thrust faults and recumbent folds (Dykstra et al., 2011). The lower part of the zone is difficult to differentiate from the upper part of the middle zone, but more or less coincides with the folded turbidite (block type c), which acts as a marker of the lower part for the upper zone. The turbidite is often mesoscopically (metre-scale) folded due to its viscosity contrast with the matrix (unlike the rafts). The blocks, being thicker, would have a larger wavelength if they were folded (Fig 17).

## 6 Discussion

Most outcrops of ancient MTDs are of a much smaller scale than those imaged in subsurface data. Even when MTDs are comparable in size, the exposed segment may only display a small window into the original MTD. While it may be difficult to link outcrop-scale descriptions with large-scale subsurface geometries, MTDs directly observed at outcrop do have the distinct advantage of enabling detailed relationships and structures to be directly observed. As such, they represent an invaluable contribution to our overall knowledge and understanding of processes that contribute to the development of MTDs.

(Alves and Cartwright, 2009; Alves, 2010) described a MTD from offshore Brazil where the deposit was divided into three distinct zones according to the distribution and sizes of blocks: a)

proximal deposits, with blocks as large as 7.5 km interpreted as mostly composed of remnant or 'in situ' blocks that comprise 0.3 to 0.4 of remobilized material; b) distal deposits, with widespread small scale rafted blocks (3 km), that comprise less than 0.2 of the remobilized material and; c) Marginal deposits, km-wide bands with small scale rafted blocks (<1km), comprising more than 0.6 of the failed material.

In the lower zone of the MTD that we describe, sandstone blocks may locally comprise up to 35% of the total deposit, with this proportion diminishing upwards. Conversely, the amount of siltstone rafts actually increases upwards as the number of sandstone blocks decreases. In conclusion, the total amount of blocks and rafts throughout the MTD comprise approximately 30% to 40% of the remobilized material. The lack of 'in situ' blocks and large (seismic) scale rafted blocks, together with the high rate of matrix disaggregation and block attenuation, all lead us to suggest that the preserved part of the deposit is at a significant distance from the slide scar. We conclude that block sizes and proportions indicate that Cerro Bola is a strike section through a distal zone of MTDII. However, it should be noted that a significant proportion of the sandstone blocks originated from the erosion of the underlying unit, and are therefore not strictly part of the failed material. The sandstone block (unlike the rafts) are therefore not truly analogous with the blocks described by Alves and Cartwright, (2009), as those in the MTD that we describe were not derived from the protolith but from the substrate (Dykstra et al., 2011).

The kinematic analysis of MTDs is complex and sometimes misleading. Fold hinge distributions are frequently considered as the most reliable estimator for palaeoslope (e.g. Strachan and Alsop, 2006; Woodcock, 1979). MTDs are usually simplified into a single-flow cell model, with a headwall domain dominated by extensional structures, a translational domain containing only limited structures, and a toe domain that is dominated by compressional structures (e.g. Bull et al., 2009; Hampton et al., 1996; Prior et al., 1984). However, the latter is clearly not the case, even in the simplest examples, where the flow ramps up onto the sea floor (e.g. Lucente and Pini, 2003).

The relationships between fold hinges and palaeoslope directions can be complicated by folds forming at different orientations, or folds detaching and rotating during translation (e.g. Alsop and Marco, 2013; Alsop et al., 2016; Farrell and Eaton, 1987). In addition, MTDs are frequently more

complex than a single-flow cell, suggesting that a multi-cell model, may be more appropriate in many cases (Alsop and Marco, 2014). In such a multi-cell model, local variations in flow would lead to second-order cells within the MTD. In such a situation, the various second-order flow cells would interact with one another, creating overprinting patterns and affecting the kinematic indicators. We suggest that each block or raft may effectively behave as a second-order cell that develops its own extensional and compressional structures. Such structures may interact with similar structures developed around neighbouring blocks. This interaction of flow around blocks may result in sand streaks that display only local kinematics linked to position on individual blocks rather than the bulk kinematics of the main flow.

Additionally, irregularities found in the basal shear surface are variously described in the literature (e.g. Omosanya and Alves, 2013) as scours (Posamentier and Kolla, 2003), glide tracks (Nissen et al., 1999), grooves (Posamentier and Kolla, 2003), striations (Gee et al., 2005), cat claws (Moscardelli et al., 2006), monkey fingers (McGilvery and Cook, 2003) and others. All those features are described as erosional and linear, and therefore indicative of flow direction. However, most of these features termed above are reported as the result of bottom gouging by a cohesive block being dragged at the base of the flow (McGilvery and Cook, 2003; Posamentier and Kolla, 2003). We suggest here that the erosional features described at the basal shear surface in Cerro Bola are grooves similar to those illustrated by (e.g. Bull et al., 2009; Posamentier and Kolla, 2003).

The analysis of multiple kinematic indicators is thus of major importance. For instance if a core were taken through an MTD, kinematic analysis could be very deceptive because most of the folds and sand streaks would relate to second-order flow cells developed around blocks and rafts which would be difficult to recognize in limited-width core.

## **7 Conclusions:**

A seismic scale outcrop located in northwest Argentina provides excellent 2D and 3D exposure through a Carboniferous MTD, enabling us to analyse and quantify in detail internal structures, flow behaviour, and strain variation. Here we demonstrate:

(i) Vertical variation through the MTD that consists of three distinct zones with transitional boundaries.

(ii) The basal shear surface is an irregular surface, where flow interacted and eroded the underlying strata. The MTD incorporated pieces of the substrate, and also show signs of developing a ramp and flat system approximately perpendicular to the flow.

(iii) Blocks and rafts are present throughout the whole MTD. Rafts are composed of siltstone and blocks consist of sandstone. Two theoretical models are proposed here for the origin of these blocks and rafts; (1) single slope failure; which can be subdivided into three scenarios 1a) erosion of underlying strata; (1b) fragmentation of the units originally embedded within the MTD protolith; (1c) a mixture of both; and (2) double slope failure; that alternatively explains the occurrence of the turbidite in the upper zone. Rafts are believed to be the least deformed component (relics) of the MTD protolith due to their compositional similarity with the matrix. The origin of the sandstone blocks by erosion is the only explanation with any physical evidence, but they could in theory still have their origin by fragmentation of the protolith.

(iv) Sandstone blocks and their surrounding matrix behave as second order cells, and develop their own extensional and compressional structures that interact with the neighbouring cells. Kinematic indicators around blocks display local regimes rather than the kinematics of the MTD as a whole.

(v) Sand streaks have their origin in the shearing of sandstone blocks (in accordance with Dykstra et al., 2011). They can be divided into blebs (more coherent bodies of sand) and stringers (less rigid and behaving like the MTD matrix). They are confined to the immediate surroundings of the sandstone blocks.

(vi) There is a large array of kinematic indicators in the MTD. However, due to the chaotic nature of the deposits, one should always use as many indicators as possible to best constrain movement. Consequently, we have used three different indicators (fold hinges, secondary fabric and block long (x) axes) to reinforce our interpretation. They constrain the direction of movement of the MTD towards NW or WNW, which corroborates previous assessments by Dykstra et al., (2011) and Milana et al., (2010).

## **Acknowledgments**

This work was carried out with support from CNPq (Conselho Nacional de Desenvolvimento Científico e Tecnológico) – Brazil, BG-Brazil and the University of Aberdeen. We would like to thank the following geologists for their support, camaraderie and countless hours of fieldwork: Claus Fallgatter, Victoria Valdez, Carla Puigdomenech, Guilherme Bozetti, Roberto Noll Filho and Arthur Giovannini, and we thank Lorena Moscardelli and an anonymous reviewer, whose constructive comments helped to improve the manuscript.

## References

- Alsop, G.I., Marco, S., 2012. A large-scale radial pattern of seismogenic slumping towards the Dead Sea Basin. *J. Geol. Soc. London*. 169, 99–110. doi:10.1144/0016-76492011-032
- Alsop, G.I., Marco, S., 2013. Seismogenic slump folds formed by gravity-driven tectonics down a negligible subaqueous slope. *Tectonophysics* 605, 48–69. doi:10.1016/j.tecto.2013.04.004
- Alsop, G.I., Marco, S., 2014. Fold and fabric relationships in temporally and spatially evolving slump systems: A multi-cell flow model. *J. Struct. Geol.* 63, 27–49. doi:10.1016/j.jsg.2014.02.007
- Alsop, G.I., Marco, S., Weinberger, R., Levi, T., 2016. Sedimentary and structural controls on seismogenic slumping within mass transport deposits from the Dead Sea Basin. *Sediment. Geol.* doi:10.1016/j.sedgeo.2016.02.019
- Alves, T.M., 2010. 3D Seismic examples of differential compaction in mass-transport deposits and their effect on post-failure strata. *Mar. Geol.* 271, 212–224. doi:10.1016/j.margeo.2010.02.014
- Alves, T.M., 2015. Submarine slide blocks and associated soft-sediment deformation in deep-water basins: A review. *Mar. Pet. Geol.* 67, 262–285. doi:10.1016/j.marpetgeo.2015.05.010
- Alves, T.M., Cartwright, J.A., 2009. Volume balance of a submarine landslide in the Espírito Santo Basin, offshore Brazil: Quantifying seafloor erosion, sediment accumulation and depletion. *Earth Planet. Sci. Lett.* 288, 572–580. doi:10.1016/j.epsl.2009.10.020
- Blair, T.C., McPherson, J.G., 1999. Grain-size and textural classification of coarse sedimentary particles. *J. Sediment. Res.* 69, 6–19. doi:10.2110/jsr.69.6
- Brodzikowski, K., van Loon, a. J., 1987. A systematic classification of glacial and periglacial environments, facies and deposits. *Earth-Science Rev.* 24, 297–381. doi:10.1016/0012-8252(87)90061-4
- Buatois, L.A., Mangano, M.G., 1995. Sedimentary dynamics and evolutionary history of a Late Carboniferous Gondwanic lake in north-western Argentina. *Sedimentology* 42, 415–436.

doi:10.1111/j.1365-3091.1995.tb00382.x

- Bull, S., Cartwright, J., Huuse, M., 2009. A review of kinematic indicators from mass-transport complexes using 3D seismic data. *Mar. Pet. Geol.* 26, 1132–1151. doi:10.1016/j.marpetgeo.2008.09.011
- Butler, R.W.H., McCaffrey, W.D., 2010. Structural evolution and sediment entrainment in mass-transport complexes: outcrop studies from Italy. *J. Geol. Soc. London.* 167, 617–631. doi:10.1144/0016-76492009-041
- Dunlap, D.B., Wood, L.J., Weisenberger, C., Jabour, H., 2010. Seismic geomorphology of offshore Morocco's east margin, Safi Haute Mer area. *Am. Assoc. Pet. Geol. Bull.* 94, 615–642. doi:10.1306/10270909055
- Dykstra, M., Garyfalou, K., Kertzus, V., Kneller, B., Milana, J.P., Milinaro, M., Szuman, M., Thompson, P., 2011. Mass-Transport Deposits: Combining outcrop studies and seismic forward modeling to understand lithofacies distributions, deformation, and their seismic expression. *SEPM Spec. Publ.* 95, 1–25.
- Fairweather, L., 2015. Mechanisms of supra-MTD topography generation and the interaction of turbidity currents with such deposits. Unpublished PhD thesis, University of Aberdeen.
- Fallgatter, C., 2015. Confined to Unconfined Deep-Water Systems of the Parana (Brazil) and Paganzo (Argentina) Basins. Unpublished PhD thesis, Universidade do Vale do Rio dos Sinos.
- Farrell, S.G., Eaton, S., 1987. Slump strain in the Tertiary of Cyprus and the Spanish Pyrenees. Definition of palaeoslopes and models of soft-sediment deformation. *Geol. Soc. London, Spec. Publ.* 29, 181–196. doi:10.1144/GSL.SP.1987.029.01.15
- Fernandez-Seveso, F., Tankard, A.J., 1995. Tectonics and stratigraphy of the Late Paleozoic Paganzo basin of Western Argentina and its regional implications. *Pet. basins South Am.* 62, 285–304.
- Garyfalou, K., 2015. Integrated analysis of mass-transport deposits: Outcrop, 3D seismic interpretation and fast fourier transform. Unpublished PhD thesis, University of Aberdeen.

- Garziglia, S., Migeon, S., Ducassou, E., Loncke, L., Mascle, J., 2008. Mass-transport deposits on the Rosetta province (NW Nile deep-sea turbidite system, Egyptian margin): Characteristics, distribution, and potential causal processes. *Mar. Geol.* 250, 180–198. doi:10.1016/j.margeo.2008.01.016
- Gee, M.J.R., Gawthorpe, R.L., Friedmann, J.S., 2005. Giant striations at the base of a submarine landslide. *Mar. Geol.* 214, 287–294. doi:10.1016/j.margeo.2004.09.003
- Gulbranson, E.L., Montanez, I.P., Schmitz, M.D., Limarino, C.O., Isbell, J.L., Marensi, S. a., Crowley, J.L., 2010. High-precision U-Pb calibration of Carboniferous glaciation and climate history, Paganzo Group, NW Argentina. *Geol. Soc. Am. Bull.* 122, 1480–1498. doi:10.1130/B30025.1
- Hampton, M.A., Lee, H.J., Locat, J., 1996. Submarine landslides. *Rev. Geophys.* 34, 33. doi:10.1029/95RG03287
- Jackson, C. a.-L., 2011. Three-dimensional seismic analysis of megaclast deformation within a mass transport deposit; implications for debris flow kinematics. *Geology* 39, 203–206. doi:10.1130/G31767.1
- Joanne, C., Lamarche, G., Collot, J.Y., 2013. Dynamics of giant mass transport in deep submarine environments: The Matakaoa Debris Flow, New Zealand. *Basin Res.* 25, 471–488. doi:10.1111/bre.12006
- Kneller, B., Dykstra, M., Fairweather, L., Milana, J.P., 2016. Mass-transport and slope accommodation: Implications for turbidite sandstone reservoirs. *Am. Assoc. Pet. Geol. Bull.* 100, 213–235. doi:10.1306/09011514210
- Lee, C., Nott, J., Keller, F., Parrish, A., 2004. Seismic Expression of the Cenozoic Mass Transport Complexes, Deepwater Tarfaya-Agadir Basin, Offshore Morocco, in: *Proceedings of Offshore Technology Conference. The Offshore Technology Conference.* doi:10.4043/16741-MS
- Limarino, C., Tripaldi, A., Marensi, S., Fauqué, L., 2006. Tectonic, sea-level, and climatic controls



- on Late Paleozoic sedimentation in the western basins of Argentina. *J. South Am. Earth Sci.* 22, 205–226. doi:10.1016/j.jsames.2006.09.009
- Limarino, C.O., Césari, S.N., Net, L.I., Marensi, S.A., Gutierrez, R.P., Tripaldi, A., 2002. The Upper Carboniferous postglacial transgression in the Paganzo and Río Blanco basins (northwestern Argentina): facies and stratigraphic significance. *J. South Am. Earth Sci.* 15, 445–460. doi:10.1016/S0895-9811(02)00048-2
- Lopez Gamundi, O., Espejo, I.S., Alonso, M.S., 1990. Sandstone composition changes and paleocurrent reversal in the Upper Paleozoic and Triassic deposits of the Huaco area, western Paganzo Basin, west-central Argentina. *Sediment. Geol.* 66, 99–111. doi:10.1016/0037-0738(90)90009-1
- Lucente, C.C., Pini, G.A., 2003. Anatomy and emplacement mechanism of a large submarine slide within a Miocene foredeep in the northern Apennines, Italy: a field perspective. *Am. J. Sci.* 303, 565–602.
- Macdonald, D.I.M., Moncrieff, A.C.M., Butterworth, P.J., 1993. Giant slide deposits from a Mesozoic fore-arc basin, Alexander Island, Antarctica. *Geology* 21, 1047–1050. doi:10.1130/0091-7613(1993)021<1047:GSDFAM>2.3.CO;2
- Maltman, A., 1984. On the term “soft-sediment deformation.” *J. Struct. Geol.* 6, 589–592. doi:10.1016/0191-8141(84)90069-5
- McGilvery, T.A. (Mac), Cook, D.L., 2003. The Influence of Local Gradients on Accommodation Space and Linked Depositional Elements Across a Stepped Slope Profile, Offshore Brunei, in: *Shelf Margin Deltas and Linked Down Slope Petroleum Systems: 23rd Annual. SOCIETY OF ECONOMIC PALEONTOLOGISTS AND MINERALOGISTS*, pp. 387–419. doi:10.5724/gcs.03.23.0387
- Milana, J.P., Kneller, B., Dykstra, M., 2010. Mass-Transport Deposits and Turbidites, Syn-to-Post-Glacial Carboniferous Basins of Western Argentina. *ISC 2010 F. Guid.* 01–88.

- Mills, P.C., 1983. Genesis and diagnostic value of soft-sediment deformation structures—A review. *Sediment. Geol.* 35, 83–104. doi:10.1016/0037-0738(83)90046-5
- Moscardelli, L., 2014. Boulders of the Vastitas Borealis Formation: Potential origin and implications for an ancient martian ocean. *GSA Today* 24, 4–10. doi:10.1130/GSATG197A.1
- Moscardelli, L., Wood, L., 2015. Morphometry of mass-transport deposits as a predictive tool. *Geol. Soc. Am. Bull.* 128, B31221.1. doi:10.1130/B31221.1
- Moscardelli, L., Wood, L., Mann, P., 2006. Mass-transport complexes and associated processes in the offshore area of Trinidad and Venezuela. *Am. Assoc. Pet. Geol. Bull.* 90, 1059–1088. doi:10.1306/02210605052
- Newton, C., Shipp, R., Mosher, D., Wach, G., 2004. Importance of Mass Transport Complexes in the Quaternary Development of the Nile Fan, Egypt, in: *Proceedings of Offshore Technology Conference. The Offshore Technology Conference.* doi:10.4043/16742-MS
- Nissen, S.E., Haskell, N.L., Steiner, C.T., Cotterill, K.L., 1999. Debris flow outrunner blocks, glide tracks, and pressure ridges identified on the Nigerian continental slope using 3-D seismic coherency. *Lead. Edge* 18, 595–599. doi:10.1190/1.1438343
- Omosanya, K.O., Alves, T.M., 2013. Ramps and flats of mass-transport deposits (MTDs) as markers of seafloor strain on the flanks of rising diapirs (Espírito Santo Basin, SE Brazil). *Mar. Geol.* 340, 82–97. doi:10.1016/j.margeo.2013.04.013
- Ponce, C., Carreras, J., Druguet, E., 2010. Development of “ lozenges ” in anastomosing shear zone networks in foliated rocks. *GEOGACETA* 207–210.
- Posamentier, H., Martinsen, O., 2011. The character and genesis of submarine mass-transport deposits: insights from outcrop and 3D seismic data. *Mass-Transport Depos. Deep. Settings SEPM Spec. Publ.* 96, 7–38.
- Posamentier, H.W., Kolla, V., 2003. Seismic Geomorphology and Stratigraphy of Depositional Elements in Deep-Water Settings. *J. Sediment. Res.* 73, 367–388. doi:10.1306/111302730367

- Prior, D.B., Bornhold, B.D., Johns, M.W., 1984. Depositional characteristics of a submarine debris flow. *J. Geol.* 92, 707–727. doi:00221376
- Ross, C.A., Ross, J.R.P., 1985. Late Paleozoic depositional sequences are synchronous and worldwide. *Geology* 194 – 197. doi:10.1130/0091-7613(1985)13<194:LPDSAS>2.0.CO
- Rygel, M.C., Fielding, C.R., Frank, T.D., Birgenheier, L.P., 2008. The Magnitude of Late Paleozoic Glacioeustatic Fluctuations: A Synthesis. *J. Sediment. Res.* 78, 500–511. doi:10.2110/jsr.2008.058
- Sobiesiak, M.S., Kneller, B., Alsop, G.I., Milana, J.P., 2016. Inclusion of Substrate Blocks Within a Mass Transport Deposit: A Case Study from Cerro Bola, Argentina, in: *Submarine Mass Movements and Their Consequences, 7th International Symposium. Advance in Natural and Technological Hazards Research*, Springer, The Netherlands. pp. 487–496. doi:10.1007/978-3-319-20979-1\_49
- Strachan, L.J., Alsop, G.I., 2006. Slump folds as estimators of palaeoslope: a case study from the Fisherstreet Slump of County Clare, Ireland. *Basin Res.* 18, 451–470. doi:10.1111/j.1365-2117.2006.00302.x
- Valdez Buso, V., 2015. The geological record of the Late Paleozoic Ice Age in Paganzo (Argentina) and Paraná (Brazil) Basins: comparison of sedimentary successions and glacial cycles. Unpublished PhD thesis, Universidade do Vale do Rio.
- Van Loon, a. J., 2009. Soft-sediment deformation structures in siliciclastic sediments : an overview. *Geologos* 15, 3–55.
- Woodcock, N.H., 1979. The use of slump structures as palaeoslope orientation estimators. *Sedimentology* 26, 83–99.
- Zapata, T.R., Allmendinger, R.W., 1996. Thrust-front zone of the Precordillera, Argentina: A thick-skinned triangle zone. *Am. Assoc. Pet. Geol. Bull.* 80, 359–381. doi:10.1306/64ED87E6-1724-11D7-8645000102C1865D

Fig 1: Simplified cartoon showing the two main types of 'Blocks' and 'Rafts' megaclasts found within the MTD.

Fig 2: a) Outline map showing the late Paleozoic sedimentary basins of South America. Red rectangle marks the study area (Modified from Gulbranson et al., 2010); b) Paleogeography of the late Paleozoic sedimentary basin of western Argentina. Study area of Cerro Bola is marked by circled 'CB' (Modified from Gulbranson et al., 2010); c) Geological Map of Cerro Bola (modified from Dykstra et al., 2011); d) Composite stratigraphic column of Cerro Bola divided into 3 glacial/deglacial cycles.

Fig 3: a, b) Examples of drop-stones found within the MTD. c) MTD matrix showing different sized rounded concretions (circled) developed on the outcrop surface. d) A concretion cut in half showing a round pebble within the concretion.

Fig 4: a) Example of a large sandstone block surrounded by MTD, where the block displays original bedding. Circled person for scale; b) Dirty sandstone block displaying eye-shaped geometry; c) Folded turbidite with its mud cap attached; d) Bedded siltstone raft with a 40 cm drop-stone, deflecting the bed below; e) Bedded siltstone raft without drop-stones; f) Massive siltstone raft sitting on top of another raft. Location of d) is boxed in red.

Fig 5: Oblique photograph looking east at Cerro Bola (above), and interpretation (below) showing the whole stratigraphy and interaction between the units. Note the erosive boundary between the MTD and the fluvio-deltaic. Location is shown on Fig. 2 C and unit legends are the same as Fig. 2.

Fig 6: a) Mosaic parallel to the inferred transport direction, showing the distribution of the sand blocks throughout the stratigraphy of the MTD. Note how the block size diminishes towards the left-

hand side (SE). Dotted lines mark the zones boundaries. Location is shown on Fig. 2 C. b) Mosaic normal to the transport direction, showing the greater amount of blocks in the lower zone of the MTD. Note the sand-rich matrix of the lower zone. Location is shown on (a) and unit legends are the same as Fig. 2.

Fig 7: a) Two siltstone rafts imbricating against two sandstone blocks. Red arrows show the inferred imbrication planes. b) Sandstone block thrusting upwards over another sandstone block. Red arrows mark the thrusting planes.

Fig 8: a, b) Examples of different sizes sand blebs; c, d) Sand stringers of different thicknesses ; e) Recumbent fold in the lower zone of the MTD. Note the sandy matrix; f) Sheath fold with elliptical closure pattern; g) Ductile-brittle fold; h) Complex folding in the upper zone of the MTDII.

Fig 9: a) Sandstone block with pinched edges and folded by the flow; b) Sandstone block sitting on top of a siltstone raft.

Fig 10: Shear lozenge, showing the result of shearing at the hinge area of a fold, where only one side of the fold survived. White box on top left hand side contains line drawing.

Fig 11: Upward intercalation of bedded muddy and silty layers in a flame shaped structure, with the crest deflected towards the NW parallel to transport.

Fig 12: a) Large scale folding above detachment zone. b) Parallel section throughout the MTD upper zone showing a series of five thrusting planes imbricating each other in the transport direction (NW). c) Photomosaic of a normal section throughout the upper zone. d) Line drawing of Fig 12 c showing a series of arcuate planes (black lines), that cut off and fold intervening strata (red lines).

Fig 13: a) Graph showing the relationship between the short axis versus long axis, black curved line mark the mean intersection of the parameters. b) Graph showing the height of sand blocks normalized from the base of the MTD (vertical axis), versus blocks aspect ratio (horizontal axis). Note that block ratios are more variable at the base (Sobiesiak et al., 2016). c) Three sandstone blocks aligned along the same horizon, and ‘frozen’ in the process of boudinage. d) Relationship between length and thickness of submarine blocks reported in the literature from both outcrop and subsurface, solid blue diamond represent blocks from this study. Modified from (Moscardelli, 2014). e) Graph illustrating height (vertical axis) versus the square root area of blocks (horizontal axis). Note how the blocks diminish in size and number upwards (Sobiesiak et al., 2016).

Fig 14: a) Proto-block ‘frozen’ in the process of being entrainment by the flow. Note that the proto-block is still attached to the underlying deltaic. b) Block spinning within the MTD demonstrating local sinistral movement.

Fig 15: Schematic cartoons illustrating two different scenarios proposed for entraining blocks within the MTD. a) Block derived from layer fragmentation during translation. b) Block derived from footwall and/or basin floor erosion. c) Turbidite originating by a secondary failure that eroded and redeposited the co-genetic turbidite on top of the MTD as upper zone. Unit legends are the same as Fig. 2.

Fig 16: a) Stereonet showing the overall attitude of soft-sediment fold hinges. Red circle highlights the isolated cluster of detached and rotated fold hinges, red dotted arrow points toward the mean transport direction of the red circle. b) Rose diagram showing the overall block long axis orientation. Dotted line points toward the mean transport orientation of the blocks. c – d) Secondary fabric showing the plotting of planes and poles and the mean pole.

Fig 17: Schematic drawing outlining the vertical variation, internal deformation features, basal interaction and related erosion of the MTD. Unit legends are the same as Fig. 2.

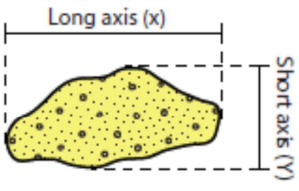
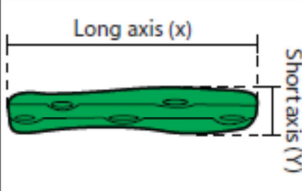
Blocks	Rafts
	
<ul style="list-style-type: none"><li>- Sandstone strata</li><li>- Highly fractured</li><li>- Shear-stripping</li><li>- Shape is variable</li><li>- Massive structures</li></ul>	<ul style="list-style-type: none"><li>- Siltstone strata</li><li>- Highly fractured</li><li>- Weakly deformed</li><li>- Rectangular shape</li><li>- Normally bedded</li></ul>

Figure 1

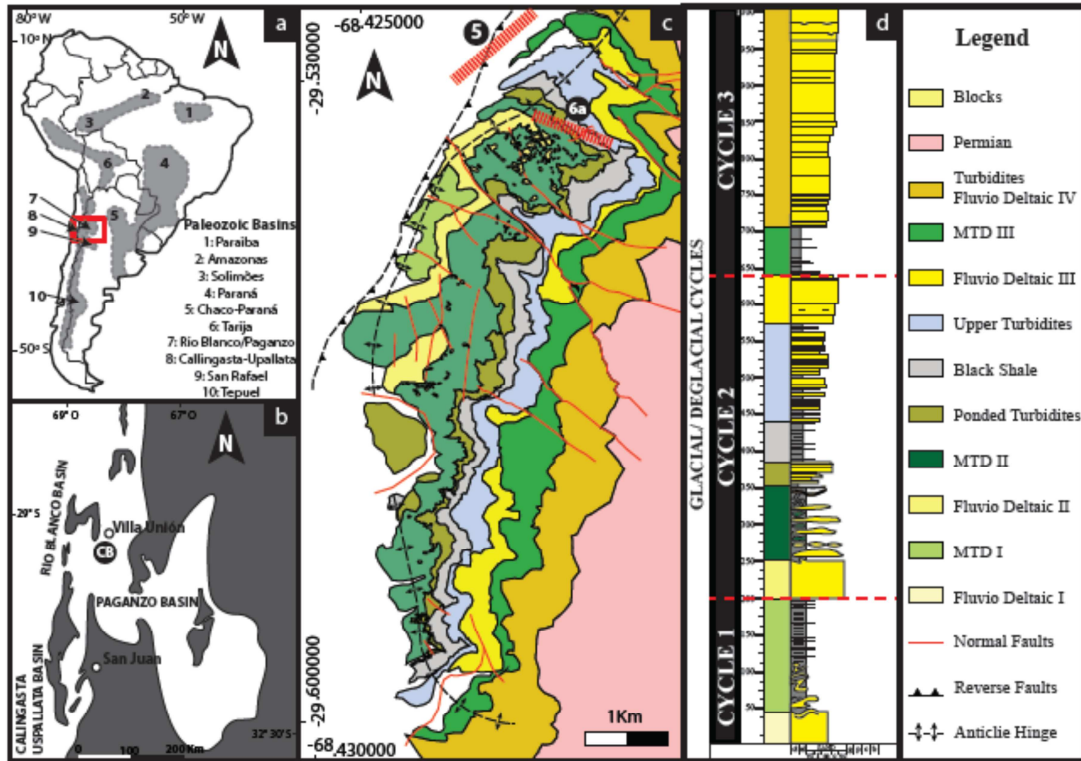


Figure 2



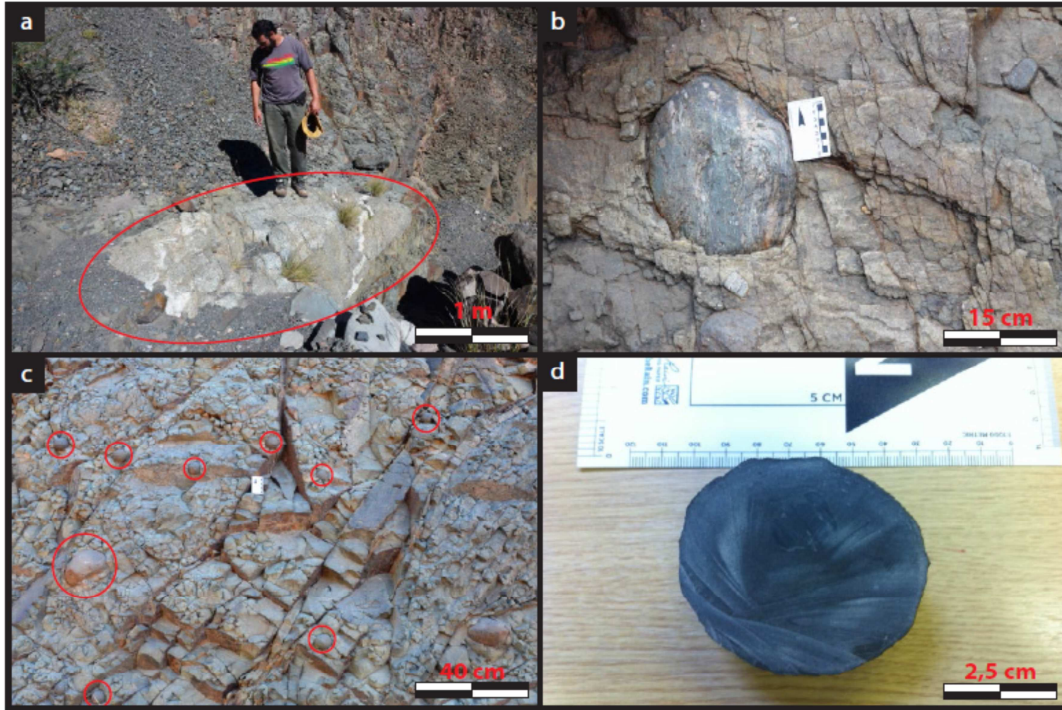


Figure 3



Figure 4



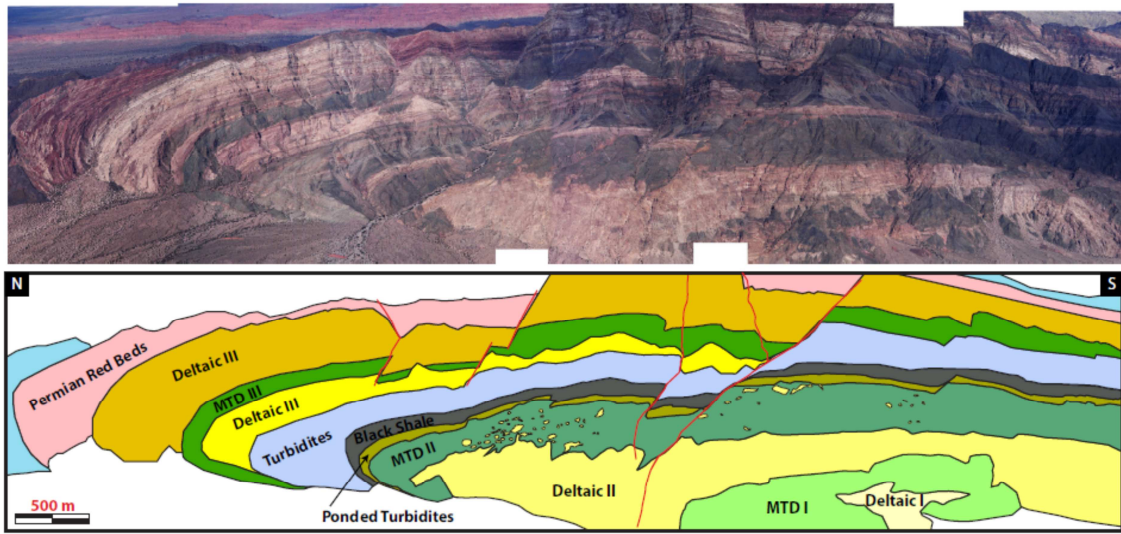


Figure 5



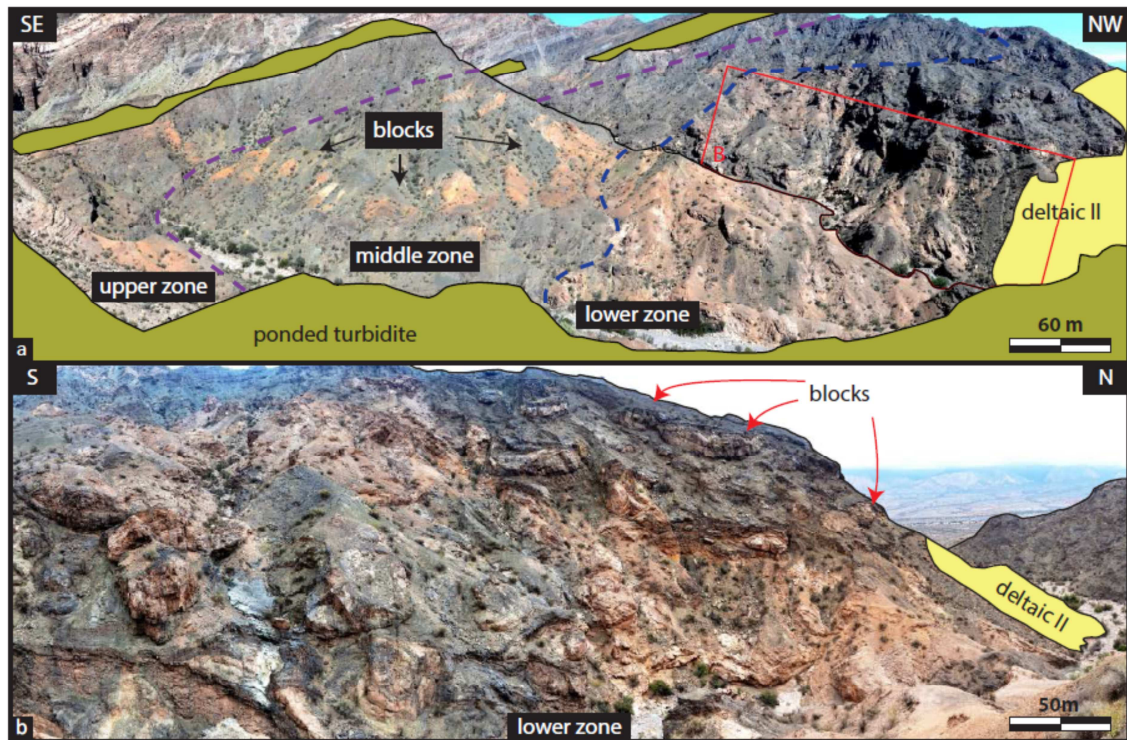


Figure 6

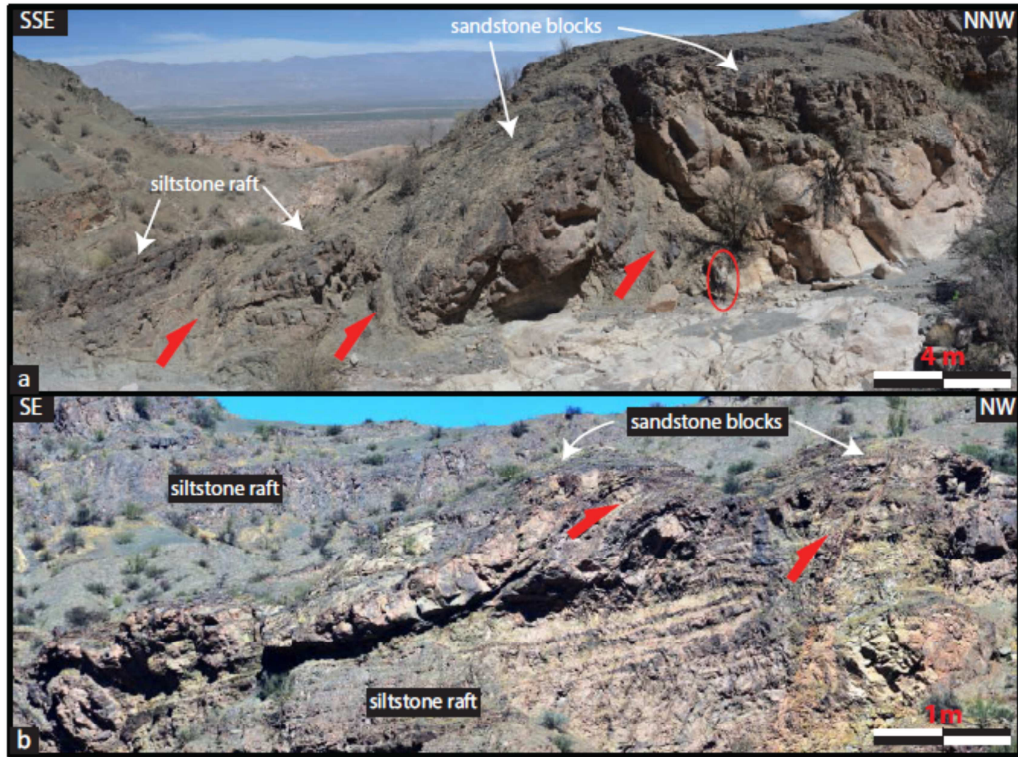


Figure 7



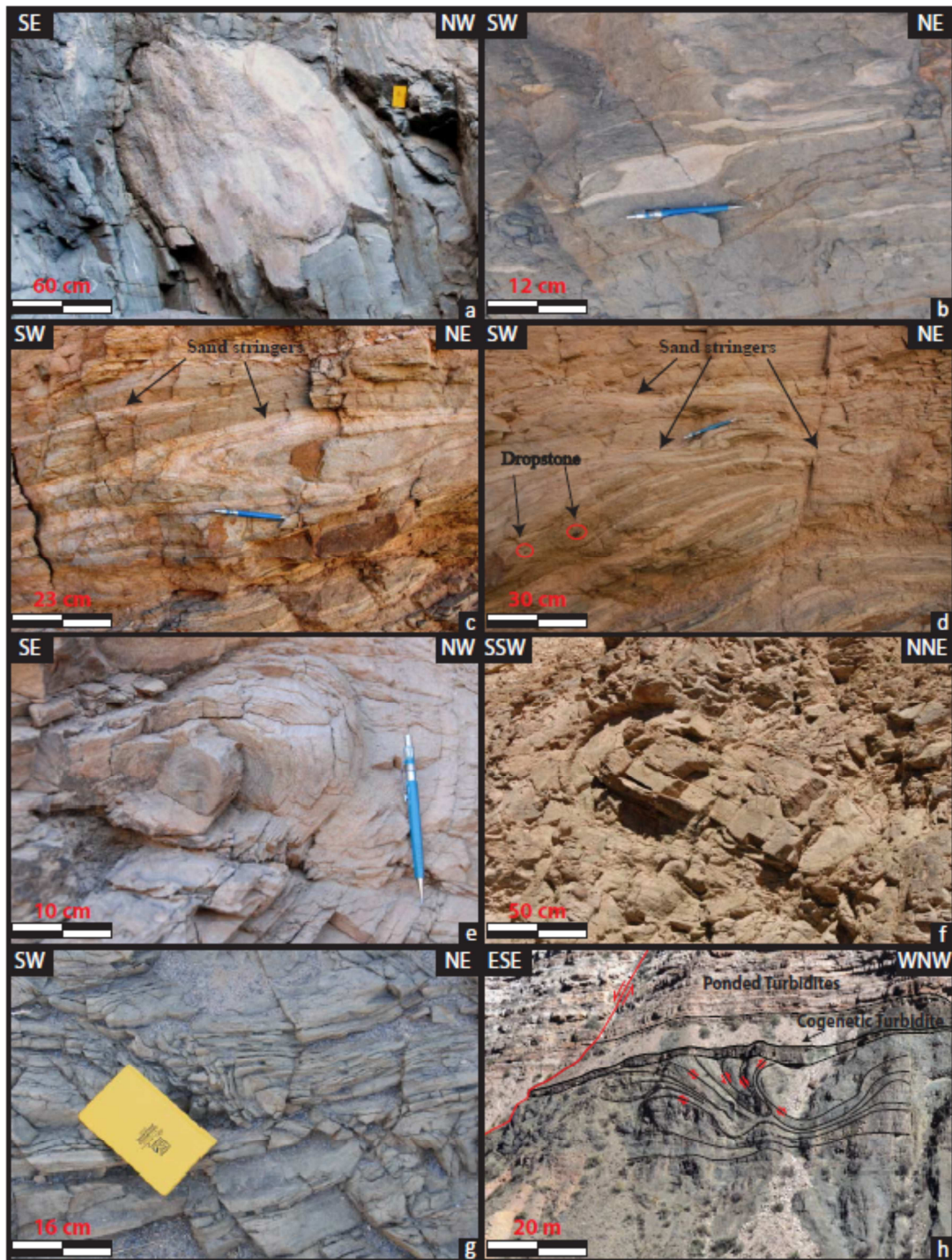


Figure 8

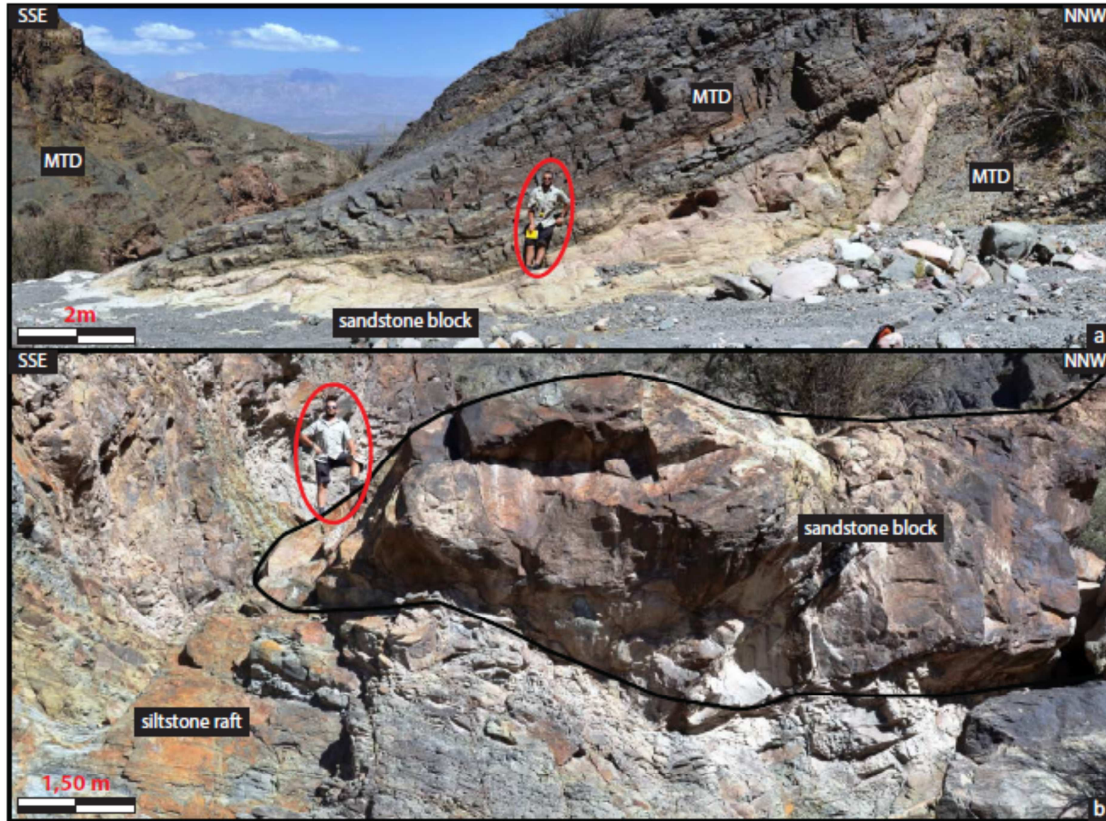


Figure 9



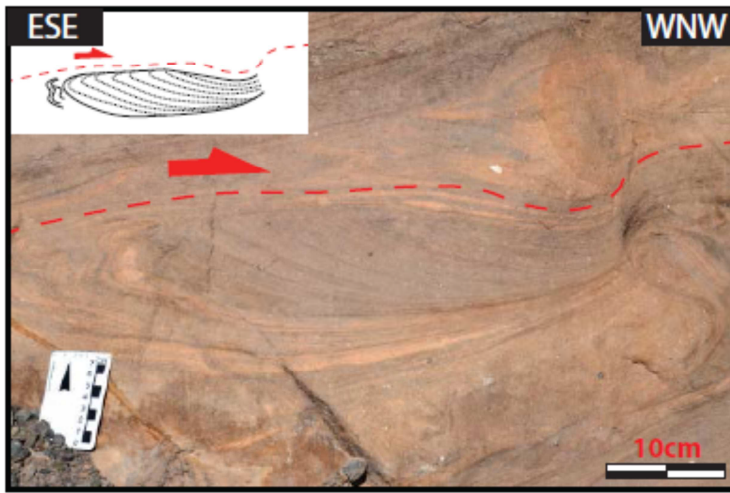


Figure 10

ACCEPTED MA



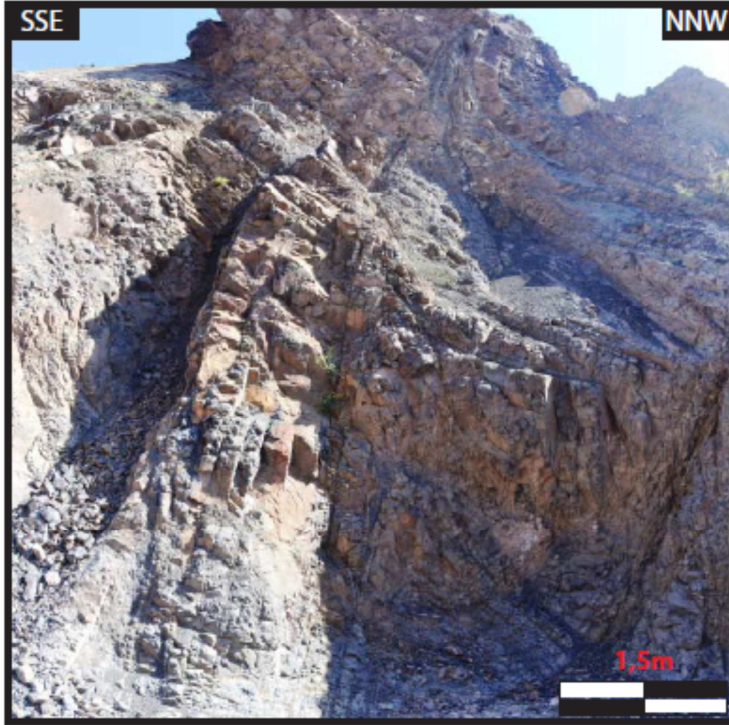


Figure 11

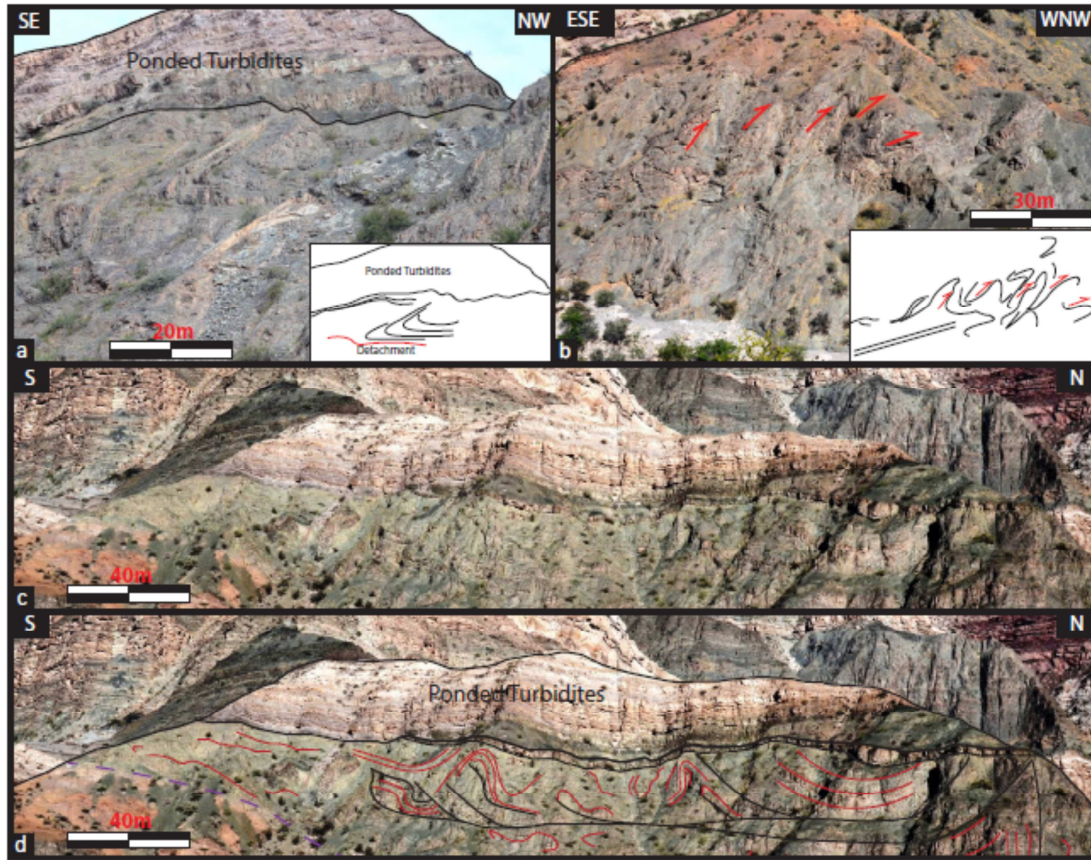


Figure 12

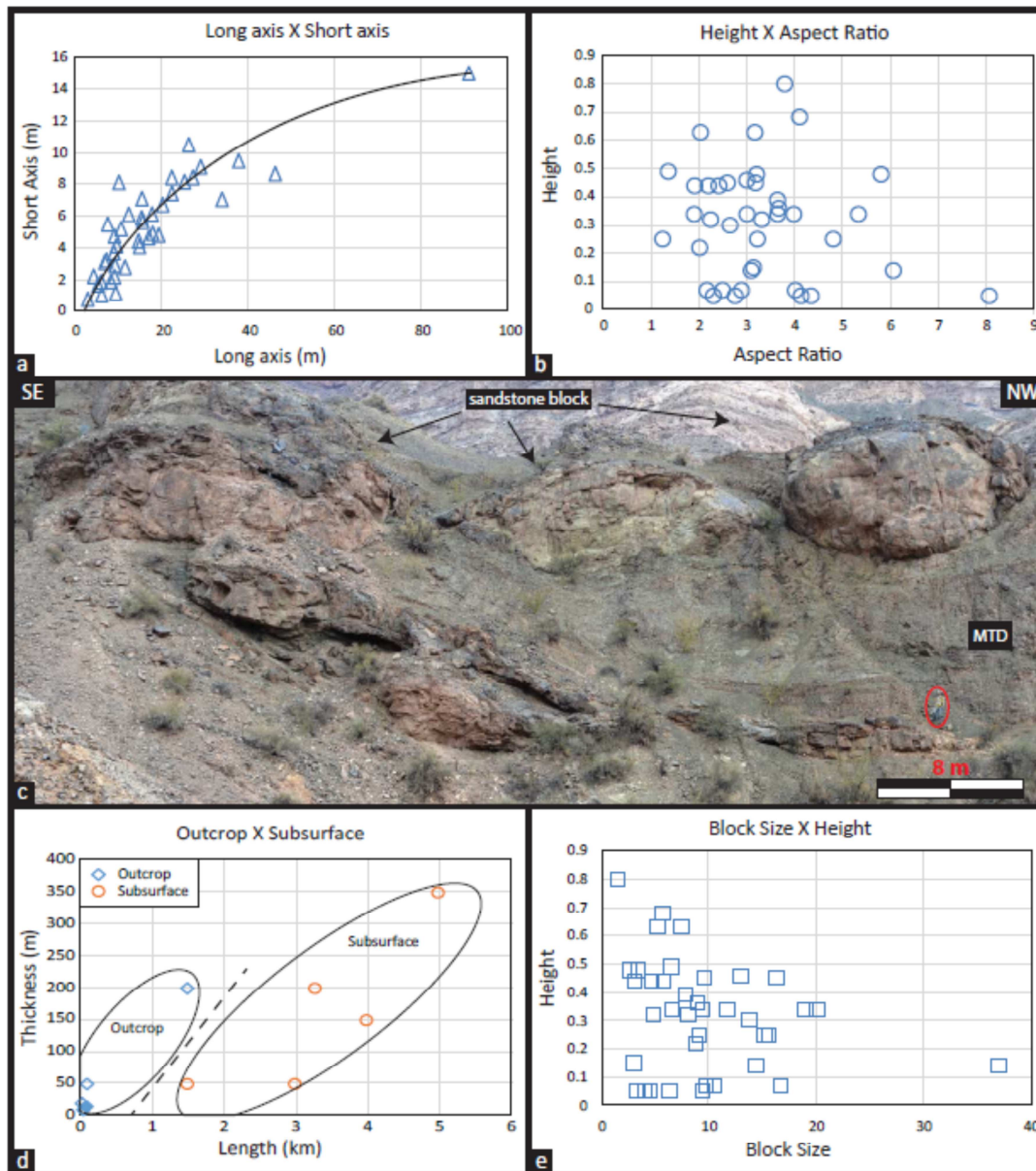


Figure 13





Figure 14

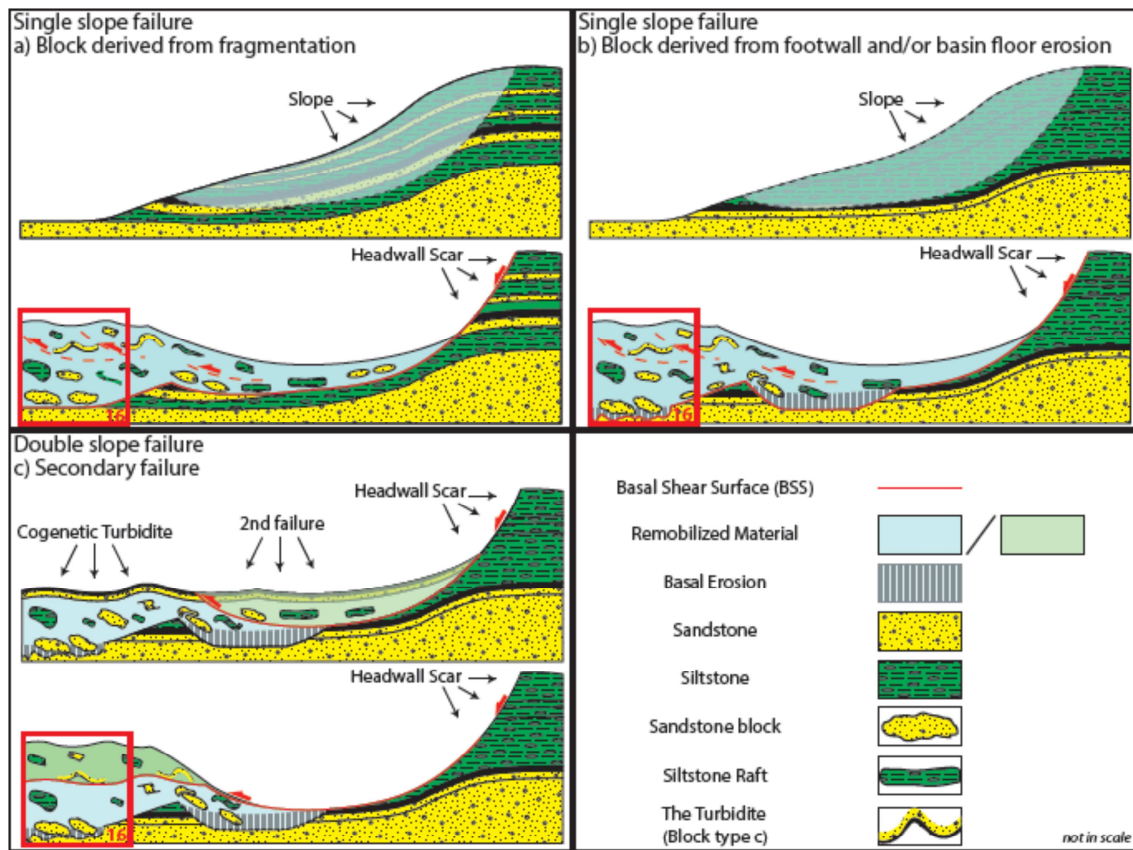


Figure 15

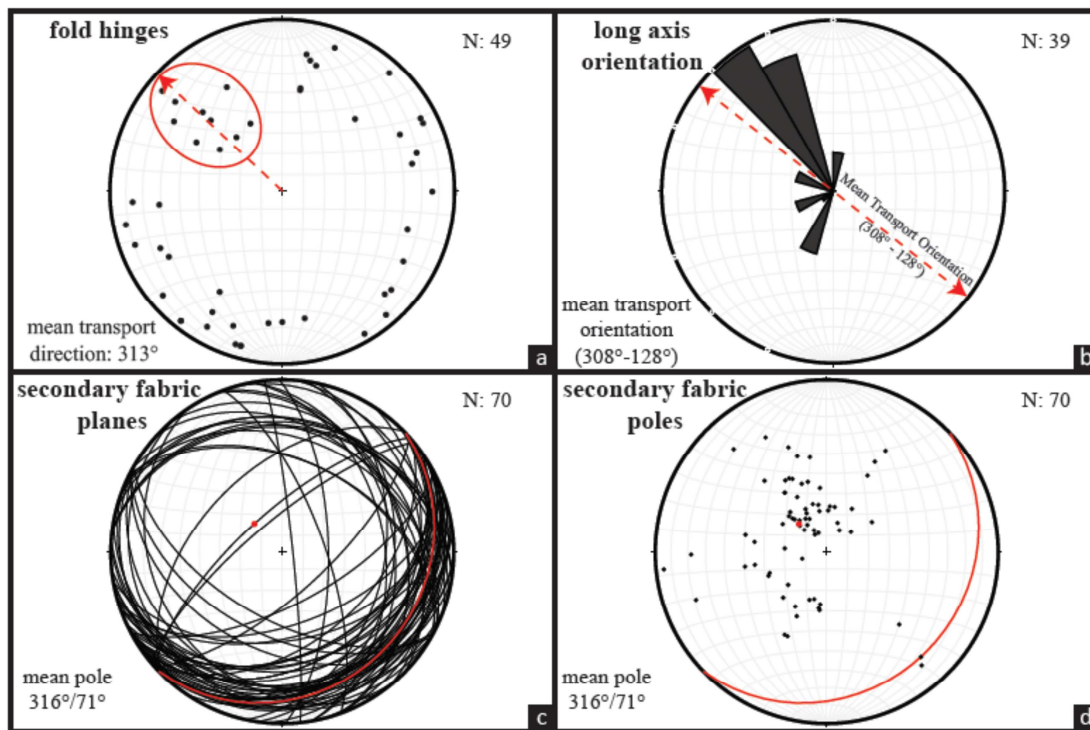


Figure 16

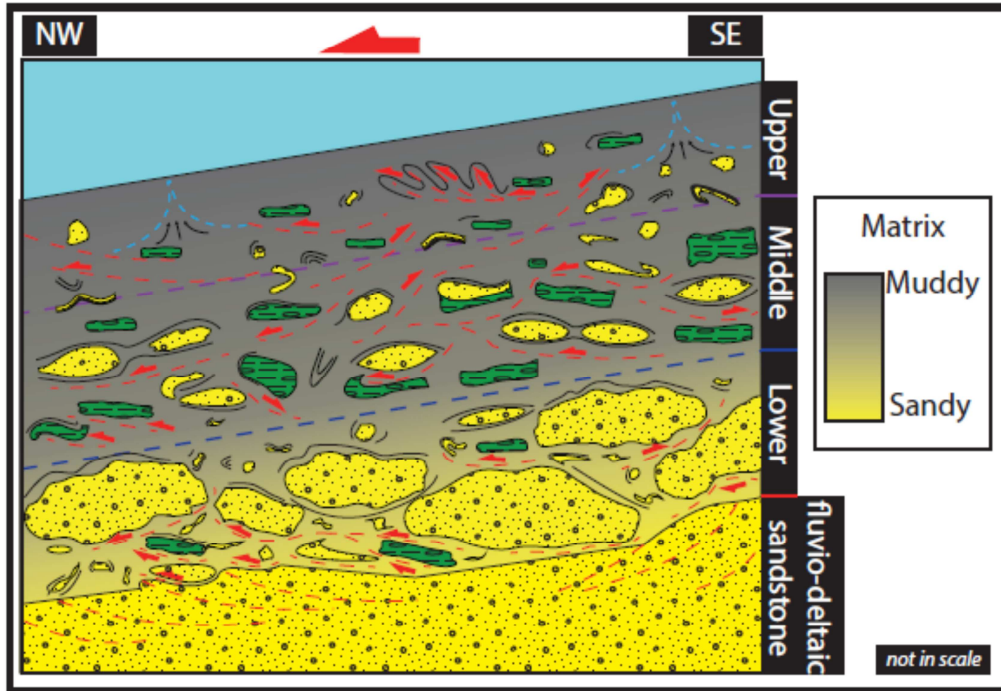


Figure 17

**Highlights**

Cerro Bola in NW Argentina provides superb outcrops through a seismic-scale MTD

The MTD is divided into 3 vertical zones based on a range of criteria

Basal shear surface is an irregular surface, where the flow interacted with the substrate.

Sandstone blocks are sheared by the flow, with sheared sand incorporated into the flow as a series of blebs and stringers.

Fold hinges, block long axes and secondary fabrics are used to constrain flow directions in the MTD.

Three theoretical scenarios are proposed to explain the failure and origin of siltstone rafts and sandstone blocks